The Black Polymorph of TTF-CA: TTF Polymorphism and Solvent Effects in Mechanochemical and Vapor Digestion Syntheses, FT-IR, Crystal Packing, and Electronic Structure

Saul H. Lapidus,[†,&] Amit Naik,[‡] Alex Wixtrom,[§] Nestor E. Massa,[ǁ] Vinh Ta Phuoc,[⊥] Leire del Campo,[#] Sébastien Lebègue,[¶,•] János G. Ángyán,[¶,•] Tarek Abdel-Fattah,[§] and Silvina Pagola*,[∇]

[†] Department of Physics and Astronomy, Stony Brook University, Stony Brook, New York 11794-3800, United States

[‡] Thomas Nelson Community College, 99 Thomas Nelson Drive, Hampton, Virginia 23666, United States

[§] Christopher Newport University, 1 Avenue of the Arts, Newport News, Virginia 23606, and Applied Research Center, 12050 Jefferson Avenue, Newport News, Virginia 23606, United States

[ǁ] Laboratorio Nacional de Investigación y Servicios en Espectroscopía Óptica-Centro CEQUINOR, Universidad Nacional de La Plata, CC962, 1900, La Plata, Argentina

[⊥] GREMAN UMR 7347, Faculté des Sciences & Techniques, Université François Rabelais Tours, Bâtiment E, 20 Avenue Monge, Parc Grandmont, 37200, Tours, France

[#] CNRS, CEMHTI UPR3079, Université d'Orléans, F-45071, Orléans, France
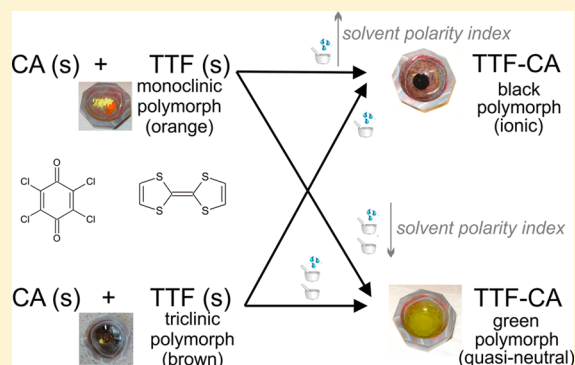
[¶] Université de Lorraine, CRM2, UMR 7036, Vandoeuvre-lès-Nancy, F-54506, France

[•] CNRS, CRM2, UMR 7036, Vandoeuvre-lès-Nancy, F-54506, France

[∇] Department of Applied Science, College of William and Mary, Williamsburg, Virginia 23187-8795, United States

Ⓢ *Supporting Information*

ABSTRACT: Tetrathiafulvalene-chloranil (TTF-CA) was synthesized by two methods, liquid assisted grinding (LAG) and vapor digestion (VD), which largely reduce the use of reaction solvents. The effects of the small quantities of LAG solvent and solvent vapors in VD toward the formation of a particular TTF-CA product polymorph were studied from both tetrathiafulvalene forms (orange and brown) as reactants. It was concluded that a high solvent polarity index favors the formation of the ionic black polymorph of TTF-CA vs the quasi-neutral green form, whereas the crystal structure and crystal habit of the orange tetrathiafulvalene polymorph also favors the formation of the black TTF-CA. The crystal structure of the black TTF-CA was determined from synchrotron X-ray powder diffraction (XRPD), and it consists of dimerized $TTF^{+\bullet}$ and $CA^{-\bullet}$ radical ions, in agreement with room temperature magnetic susceptibility measurements indicating the material is diamagnetic. FT-IR showed that the compound is a semiconductor with a small band gap of ~0.198 eV and it remains ionic at low temperatures. The latter was confirmed by XRPD showing the black TTF-CA does not undergo a phase transition in the range 298−20 K. Band structure calculations are in good agreement with the measured band gap.

INTRODUCTION

Polymorphism studies are very important in various fields such as pharmaceutical solids, agrochemicals, pigments and high energy materials.[1] The differences in bulk physical properties (e.g., electrical conductivity, magnetic properties) observed in polymorphic modifications of charge transfer salts (CTS) of the electron donor tetrathiafulvalene (TTF) are noteworthy. Most organic solids are electrical insulators[2] with electrical conductivities in the order of 10^{-20} to 10^{-15} Ω^{-1} cm^{-1}. CTS of TTF are an interesting class of materials that can give rise to organic conductors. Columnar stacks of TTF molecules in the crystal structure leading to a conduction path for π electrons,

plus partially filled electron energy bands due to a partial charge transfer between TTF (electron donor) and electron acceptors, are the structural and band structure requirements for the formation of TTF-based organic metals.[1−3] The tetrahalo-*p*-benzoquinones fluoranil (FA), chloranil (CA), bromanil (BA) and iodanil (IA) are electron acceptors that form CTS with TTF. However, all of their reported 1:1 molar ratio crystal structures are composed of stacks showing alternating electron

donor and acceptor molecules[4−6] also, in general, regarded as thermodynamically more stable than the packing motif mentioned above.[1]

CTS with partial charge transfer are labeled 'quasi-neutral' (ρ < 0.5) or 'quasi-ionic' (ρ > 0.5), where ρ is the degree of ionicity. TTF-tetrahalo-p-benzoquinone structures show another interesting phenomenon under temperature decrease or pressure increase: TTF-CA[7−9] and TTF-IA[10] undergo a neutral to ionic phase transition accompanied by an increase in ρ. TTF-BA is ionic at all temperatures.[6,11]

Two polymorphs of TTF-CA have been reported in literature, the green and black forms.[4,8,12,13] The green form, quasi-neutral at room temperature (RT), has been extensively studied,[1] and it is a prototype material for understanding the neutral to ionic transition in one-dimensional TTF-based CTS.[8,14] Although early FT-IR studies indicated that the black polymorph of TTF-CA is an ionic phase (thus not an organic metal), made of TTF and CA dimers,[13] its crystal structure and physicochemical properties have remained elusive until this work.

We have synthesized the black polymorph of TTF-CA by mechanochemistry and by vapor digestion (VD). Both synthetic methods have the economical and environmental advantages of avoiding or largely reducing the use of solvents, thus providing *"green chemistry"* synthetic alternatives. Grinding the reactants in a mortar with a pestle or ball mill together with small quantities of solvents, called solvent drop grinding,[15] kneading,[16] liquid assisted grinding (LAG),[17,18] or solvent assisted mechanochemistry (SAM),[19] usually yields products of increased crystallinity,[17,18] can enable mechanochemical reactions,[16−18] increase the reaction rates,[15−20] and lead to the selective formation of particular product polymorphs.[16−20] More recently, 'solvent drop grinding' has been replaced by LAG, and thus, a solvation role of the liquid phase is not assumed *a priori*.[16]

The most commonly used method for the synthesis of CTS is electrocrystallization.[1] Our work shows that LAG is also a promising synthetic method for polymorph screening of TTF-based CTS. This is significant as the control of the experimental conditions leading to a particular polymorph and avoiding others can be a challenge in the CTS field.[1] Moreover, occasionally mechanochemical reactions afford products or stoichiometries not obtainable from solution chemistry;[19,20] thus, additional CTS polymorphs could have been revealed by LAG. A disadvantage of LAG is that the products obtained are powders rather than single crystals, thus precluding the anisotropic study of physicochemical properties. However, TTF-CA products were sufficiently crystalline to allow for crystal structure determination from powder diffraction.[16,21,22]

In VD syntheses, the reactants are exposed to solvent vapors for a relatively long period (10 days in this study), which leads to a chemical reaction. In order to gather experimental observations toward understanding the role of the solvent in LAG and VD syntheses of TTF-CA and gain further insights into the possible mechanisms of this reaction, we have determined the particular polymorph obtained by neat grinding, LAG and VD from both TTF polymorphs, the brown (triclinic form) and the orange (monoclinic form), using a series of solvents of decreasing polarity index: water, dimethyl sulfoxide (DMSO), acetonitrile (MeCN), acetone, ethyl acetate and toluene, since one of the TTF-CA products is ionic and the other is quasi-neutral at room temperature.

■ EXPERIMENTAL SECTION

Synthetic Procedures and Materials. TTF (99% purity) was obtained from Sigma-Aldrich (brown, triclinic polymorph) and from Acros Organics (orange, monoclinic polymorph). CA (99% purity), and solvent reagents were obtained from commercial suppliers and used as received. The sample of TTF-CA black polymorph used for synchrotron XRPD was synthesized by LAG, manually grinding 0.0227 g (1.11×10^{-4} mol) of TTF (orange form) and 0.0273 g (1.11×10^{-4} mol) of CA in an agate mortar with pestle for 25 min under air in the presence of 4 drops (∼70 μL) of DMSO added at the start of the grinding process. The sample used for FT-IR analysis was synthesized by LAG with water for 30 min under air using 0.0454 g (2.22×10^{-4} mol) of TTF (brown form) and 0.0546 g (2.22×10^{-4} mol) of CA. One hundred microliters of water were added immediately before the start of grinding, and an additional 100 μL were added 20 min after the start. The sample for magnetic susceptibility was prepared by LAG for 30 min under air 0.0454 g of TTF (orange) and 0.0546 g of CA, with 5 μL of DMSO, added at the start of the LAG reaction.

The syntheses to study the effect of the solvent in LAG using the brown and orange TTF forms were carried out by grinding for 30 min under air using 0.0113 g (5.55×10^{-5} mol) of TTF and 0.0136 g (5.55×10^{-5} mol) of CA, with 50 μL of MeCN, acetone, toluene or ethyl acetate added to the reactant mixture immediately before the start of grinding, and 50 μL added again 15 min after the beginning of the mechanochemical reaction. Neat grinding reactions from each TTF polymorph were also performed using the TTF and CA masses above. To study the effects of the solvent quantity in product polymorph control by LAG, a larger number of syntheses were done from each TTF polymorph using increasing quantities of water and DMSO. Those additional synthesis conditions are detailed in the Supporting Information (SI) file.

For the VD syntheses of TTF-CA, 0.0102 g (5.0×10^{-5} mol) of TTF and 0.0123 g (5.0×10^{-5} mol) of CA were placed in glass vials and gently mixed with a spatula. Brown and orange forms of TTF (not ground) were tried separately. Micrographs indicating typical crystallite dimensions are shown in the SI file (Figures S2c and S5c). Each vial was placed in a glass jar with lid, together with another vial containing 5−10 mL of one of the following solvents: water, DMSO, acetone, ethyl acetate, or toluene. The glass jars were purged with N_2 for 5 min, tightly closed and covered with Al foil. Each vial was recovered from the sealed glass jar after 10 days at 295 K.

FT-IR and Magnetic Susceptibility Measurements. Two mass magnetic susceptibility measurements were carried out in a Johnson Matthey, U.S.A., balance. The balance was calibrated with a Hg[Co(SCN)$_4$] standard. Temperature-dependent Fourier transform far-infrared (FIR) and mid-infrared (MIR) measurements were collected in a Bruker 66 V interferometer with 2 cm^{-1} resolution at RT and 10 K. Pellets made of TTF-CA microcrystals diluted in KBr (for MIR) or polyethylene (for FIR), were mounted on the coldfinger of a He closed-cycle cryostat.

X-ray Powder Diffraction. The synchrotron XRPD patterns of TTF-CA (black form) were collected at RT and at 20 K, in transmission geometry from a glass capillary at λ = 0.699931 Å, at the beamline X16C, N.S.L.S., Brookhaven National Laboratory, U.S.A. The wavelength was selected with a Si(111) double monochromator and the incident parallel beam was monitored with an ion chamber. A Ge(111) analyzer crystal was placed after the sample and before the detector to obtain good angular resolution, whereas the out-of-plane resolution was given by slits. A NaI(Tl) scintillation detector was used to measure the diffracted radiation. For data collection at 20 K, the sample was mounted in a He closed-cycle cryostat.

The RT pattern has been previously indexed with the program ITO.[23] The lattice parameters refined for this specimen are equivalent to the ones previously found[24] within reasonable error limits. A preliminary crystallographic model was obtained with the program PSSP,[21] and it was confirmed and improved with the program TOPAS.[22] The Rietveld refinement reported was carried out with the program GSAS,[25] using soft bond length, bond angle and planarity restraints. After the observation of average preliminary refined values
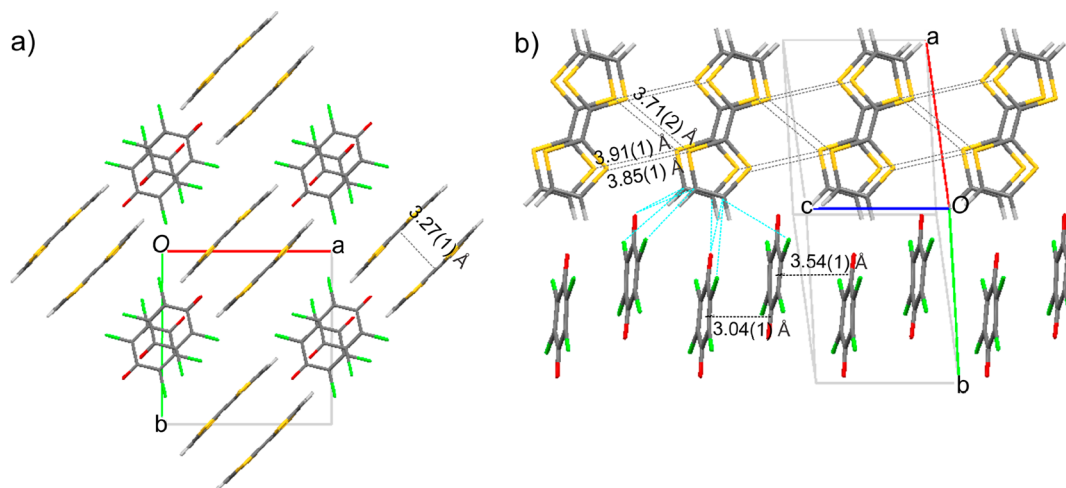
Figure 1. Crystal packing of the TTF-CA black polymorph at RT. (a) View along [001] showing eclipsed $(TTF^{+\bullet})_2$ dimers. (b) View approximately along [110] showing columns of TTF and CA dimers. (C: gray, S: yellow, Cl: green, O: red, and H: light gray). Selected nonclassical (weak) hydrogen-bonding distances as found by PLATON,[35] and S···S noncovalent interactions are shown with light-blue and gray dashed lines, respectively.

of bond lengths in both five-member rings of TTF, the bond length restraints were tightened from the softer values used in the stage above, to promote slightly shorter and larger bond distances (on average) in both rings of TTF, simulating aromatic and nonaromatic bonding. The restraints values were taken from the TTF geometry in the quasi-ionic TTF-CA, which was determined by single-crystal neutron diffraction.[8] The isotropic thermal displacement parameters of the non-H atoms of TTF and CA molecules were refined using two group constraints, whereas those of the H atoms were constrained to 1.2 times the value refined for the non-H atoms of TTF. The standard uncertainties of the atomic coordinates and thermal displacement parameters were corrected using the procedure described by Scott.[26] The crystal structures were represented with the program Mercury version 3.1.[27]

Laboratory XRPD data was collected in a Rigaku Miniflex II in reflection geometry using Cu Kα radiation (λ = 1.5418 Å). The samples were loaded in zero background sample holders made of quartz, and the data were collected in the 2θ interval 5°−65°, using 0.02° step size and 1°/min scan speed.

Computational Techniques. The band structure calculations were performed using the HSE06 hybrid functional approximation.[28−30] The exchange potential contains a part of the Hartree−Fock potential for the short-range part of the interaction, while the correlation potential is kept at the generalized gradient level (GGA).[31] The HSE06 functional is known to solve at least partly the problem of self-interaction, and it provides band-gaps usually in much better agreement with experiments than the GGA.[32] The projector augmented wave method,[33] as implemented in the Vienna *Ab initio* Simulation Package (VASP),[34] has been used. Lattice parameters and the non-hydrogen atom positions were taken from the RT synchrotron XRPD results, while the positions of the hydrogen atoms were optimized. To ensure convergence, a 4 × 4 × 2 k-point mesh was used to sample the Brillouin zone together with the default cutoff for the plane-wave expansion.

■ RESULTS AND DISCUSSION

Crystal Structure Analysis and Room Temperature Magnetic Susceptibility. The crystal structures of TTF-CA (black form) at RT and 20 K, were determined from their synchrotron XRPD patterns. Figure 1 shows the crystal structure at RT, and the Rietveld graph is shown in the SI file (Figure S7).

As previously determined from the analysis of infrared measurements,[13] this material is composed of TTF dimers

easily discerned along [001]. The TTF units in the dimers are planar and in an eclipsed configuration, with an interplanar TTF−TTF distance of 3.27(1) Å, in agreement with values found in the Cambridge Structural Database[36] for TTF compounds that contain $(TTF^{+\bullet})_2$ radical cation dimers. The $TTF^{+\bullet}$ radical cation is generated when one of the dithiolylidene rings in TTF becomes aromatic by losing one electron.

Viewed along [001] the dimers in TTF-CA appear isolated; however, the view along [110] in Figure 1b shows that they are actually part of columns running along [001]. The orientation of the dimers with respect to each other within the column precludes the overlap of the π systems of neighbor dimers. However, there are S···S noncovalent contacts between dimers along the column at distances of 3.71(2) Å, 3.91(1) Å and 3.85(1) Å. Moreover, it is known that a strong two-electron bond of σ type is formed in the eclipsed (and ionic) dimeric radical cation $(TTF^{+\bullet})_2$ units,[37] which gives rise to diamagnetic and semiconductor/insulating properties. This packing motif is not observed in mixed-valence TTF-based organic metals, which show bond-over-ring overlap of TTF units in infinite one-dimensional columnar stacks.[1,37]

Figure 1b shows also dimerized columns of CA running along [001], with interplanar short and long CA−CA distances of 3.04(1) Å and 3.54(1) Å, respectively. CA molecules are not stacked in an eclipsed configuration, and their centroid−centroid distances are 3.65(1) Å and 3.86(1) Å, with slippage distances of 2.03 Å and 1.52 Å, respectively; thus, the packing in the column rather resembles a bond-over-ring type (see Figure 1a).

Tetrahalo-*p*-benzoquinones form stable radical anions wherein the aromaticity of the ring is increased in comparison to quinones, though the molecular geometry is more similar to a quinone than to a hydroquinone (aromatic).[38] Diamagnetic dimeric species of radical anions are stabilized by spin coupling of unpaired electrons of adjacent rings. The crystal structures of three acetone solvates of potassium and rubidium salts of tetrachlorosemiquinone and potassium tetrabromosemiquinone contain columns of π-stacked radical anion dimers[38] similar to the ones found in TTF-CA (black polymorph).

Moreover, in the black polymorph of TTF-CA the columnar arrays of TTF and CA units are linked by multiple weak (nonclassical) hydrogen bonds between H atoms of TTF, O and Cl atoms of CA, and these are shown in Figure 1b. In agreement with the crystal structure and the chemical bonding in the $(TTF^{+\bullet})_2$ and $(CA^{-\bullet})_2$ dimers, the black form of TTF-CA was experimentally found to be diamagnetic with RT mass magnetic susceptibility of $-(0.24 \pm 0.03) \times 10^{-6}$ cm^3/g.

We have also noted that the crystal structure of TTF-CA above resembles the one depicted for another ionic and diamagnetic charge transfer salt, TTF-DDQ (DDQ = 2,3-dichloro-5,6-dicyano-p-benzoquinone),[39] although its coordinates were not found in the Cambridge Structural Database.[36] The DDQ molecules were reported to be disordered with partial exchange of −CN and −Cl substituents. The lattice parameters refined were $a = 10.227(4)$ Å, $b = 12.195(5)$ Å, $c = 6.609(2)$ Å, $\alpha = 77.51(2)°$, $\beta = 81.93(2)°$, $\gamma = 87.30(4)°$, and $Z = 2$ in $P\bar{1}$. The values of a, b, and c above are comparable to the ones of TTF-CA (black polymorph) shown in Table 1, and

Table 1. Crystal Data of the Black Polymorph of TTF-CA ($C_{12}S_4H_4Cl_4O_2$, $M_r = 450.23$) at RT and 20 K

data collection temperature	298 K (RT)	20 K
space group	$P\bar{1}$	$P\bar{1}$
Z	2	2
D_x (g/cm^3)	1.944	1.997
radiation	Synchrotron, $\lambda = 0.699931$ Å	Synchrotron, $\lambda = 0.699931$ Å
R_{wp} (%)	5.84	12.95
R_I (%)	2.95	6.49
χ^2	1.80	1.34
a (Å)	10.7692(3)	10.7378(6)
b (Å)	11.0465(3)	10.9492(6)
c (Å)	6.6085(1)	6.4879(3)
α (deg)	101.356(3)	100.481(6)
β (deg)	93.669(2)	93.069(6)
γ (deg)	89.295(1)	89.954(2)
V (Å^3)	769.19(3)	748.95(7)

from Figure 2 in ref 39 it seems that the compounds are isostructural. The authors report intra- and inter-DDQ dimer distances of 3.0 Å and 3.56 Å, respectively,[39] and interplanar spacing between eclipsed TTF molecules of 3.4 Å, essentially equivalent to the values refined for CA dimers (3.04(1) Å and 3.54(1) Å, respectively) and in good agreement with the value for TTF dimers (3.27(1) Å).

Furthermore, one-dimensional structures are intrinsically unstable for thermodynamic reasons.[14] CTS often display ordering phenomena giving rise to phase transitions as a function of the temperature, pressure, or an order parameter in general, which break the symmetry of the lattice, charge, or spin degrees of freedom.[14] To investigate the presence of crystallographic phase transitions in this TTF-CA polymorph, we have also studied its crystal structure at 20 K. The analysis of the synchrotron XRPD data indicates that a crystal phase transition is not observed, and the Rietveld fit at 20 K is shown in Figure S8 SI. The lattice parameter variation is less than 1% in all cases, except for the c-axis which is ∼2%.

We have calculated the inter- and intradimer distances in $(TTF^{+\bullet})_2$ and $(CA^{-\bullet})_2$ at 20 K, which are 3.300(9) Å, 3.00(1) Å and 3.46(1) Å, also showing that the packing is essentially

unchanged. The TTF and CA intradimer distances have changed ∼1%, and the CA interdimer distance, ∼2%.

After comparison of the densities of the black (ionic), green (quasi-neutral) and quasi-ionic TTF-CA at RT and low temperatures, we observe that the black form of TTF-CA is the densest polymorph at all temperatures. The (green) quasi-neutral TTF-CA has a density of 1.841 g/cm^3 at RT, and the pseudoionic TTF-CA has a density of 1.932 g/cm^3 at 40 K. For the black TTF-CA the densities are 1.944 g/cm^3 at RT and 1.997 g/cm^3 at 20 K. Following the density rule,[1,40] this indicates a larger thermodynamic stability for the ionic TTF-CA. Table 1 summarizes the crystallographic results for TTF-CA (black polymorph) at RT and 20 K.

Moreover, sometimes mechanochemical reactions yield products not obtainable from solution chemistry. In this system, a hypothetical mixed valence and potentially conducting structure with segregated TTF and CA stacks, in general considered thermodynamically less stable than the alternated stacks packing (e.g., green TTF-CA polymorph),[1] has not been found experimentally, using either LAG or VD syntheses.

FT-IR Spectroscopy, Band Gap and Electronic Structure Calculations. We have carried out FT-IR studies of the black polymorph of TTF-CA to investigate experimentally the presence of a band gap. The FT-IR spectrum of TTF-CA (black form) at RT in transmission mode is shown in Figure 2. The spectrum is essentially equivalent to the one
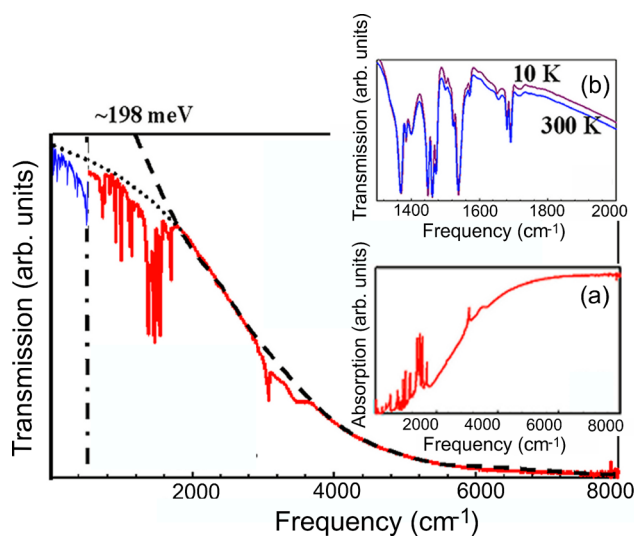

Figure 2. Room temperature FT-IR transmission spectrum of TTF-CA (black form). The blue line at the left-hand side of the vertical point-dashed line shows the FIR spectrum from polyethylene pellets. The red line at the right-hand side shows the MIR spectrum from KBr pellets. The TTF-CA band gap corresponds to the extrapolation of the dashed line at ∼198 meV. The baseline delineated in dots is the consequence of states in the gap. (a) Overall view of the TTF-CA absorption edge. (b) Transmission spectra showing mostly identical vibrational band profiles at RT and 10 K.

published in 1983 by Girlando et al.,[13] corresponding to an ionic compound. The detailed phonon structure shows subtle differences, and splitting in bands is most likely due to the higher resolution of our modern instrument. However, we have noted a group of bands at around 1700 cm^{-1} not reported in that work, but that were consistently found in our spectra from samples of which purity was previously checked by XRPD.

There is a sharp increase in the absorption at around 1000 cm^{-1} (Figure 2a, inset) that can be associated to a band gap of ~198 meV. The baseline at lower frequencies in the transmission spectrum shown in Figure 2 suggests that the black form of TTF-CA is not a clean insulator since it has a tail shape characteristic of dirtier gaps. We hypothesize that the origin of the levels within the gap is likely due to dangling bonds in an imperfect lattice topology, which may also contribute to vibrational band broadening. The spectra at RT and 10 K shown in Figure 2b, inset) are basically equal; thus, the ionicity and electrical conductivity properties do not change considerably in this temperature range. At 10 K, there is a small reduction in absorption, most likely due to temperature-driven carrier localization that does not alter the overall picture of TTF-CA (black form) as an ionic compound. These results are consistent with the XRPD results at 20 K, which indicate that the material does not undergo a crystal phase transition in the temperature range 298−20 K.

The above experimental value of the band gap has been confirmed through density functional theory (DFT) band structure calculations using the Heyd−Scuseria−Ernzernhof (HSE06) exchange-correlation potential in the hybrid functional approximation.[28−30] The calculated band structure, as shown in Figure 3a, has a minimum indirect band gap of 0.08 eV between the Y and Γ high-symmetry points. The corresponding total density of states (DOS) shown in Figure 3b confirms the value given above for the band gap. The minimum direct ban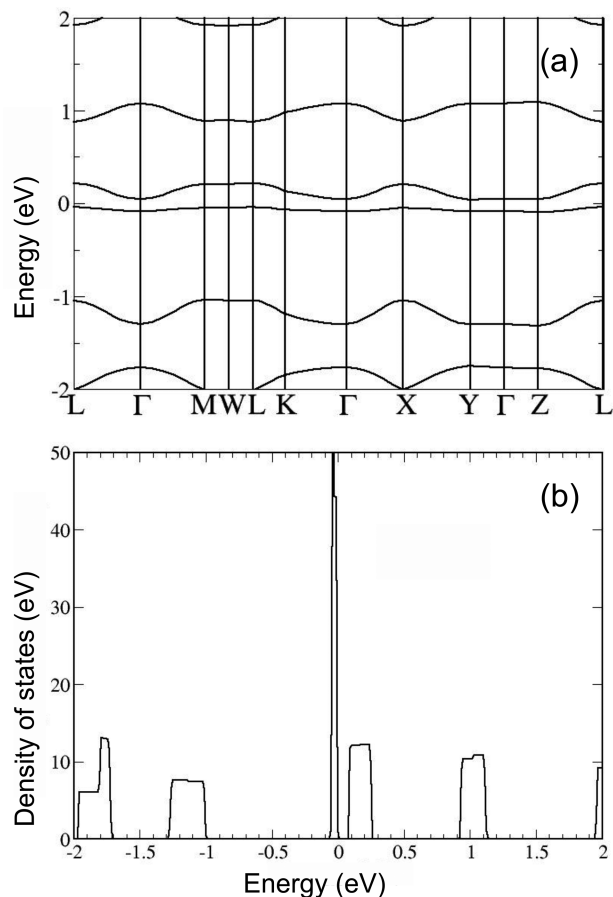d gap of 0.12 eV is observed at the Y high-symmetry point, albeit it is almost degenerated with the direct band gap at the Γ point.

In order to understand how the molecular states are distributed in energy in the DOS, we have summed up the partial DOS for each atom that belong to either TTF or CA molecules in the crystal. The states immediately below the Fermi level (which is placed at zero eV), are from the CA units (see Figure 3b and Figure 4a for comparison), while the states
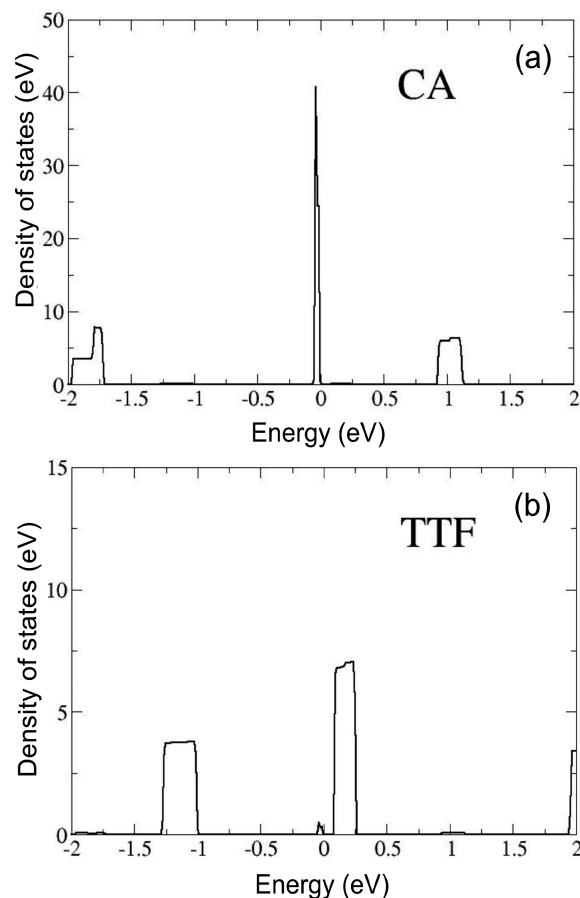

Figure 4. (a) Density of states contributed by: (a) CA molecules, and (b) TTF molecules.

Figure 3. (a) Band structure calculation, and (b) total density of states of TTF-CA (black polymorph).

immediately above (Figures 3b and 4b) are from the TTF molecules. The calculated band gap is in very good agreement with the experimental value obtained by FT-IR measurements.

TTF Polymorphism and Solvent Effect in LAG and VD Syntheses. Mechanical processes such as grinding add mechanical energy to a chemical system, increasing lattice imperfections and the reactivity of species. The accumulated energy can relax physically by emission of heat or through chemical processes.[41−43] Mechanical action also increases the surface area of solids, forming fresh interfaces between reactants that facilitate the diffusion of species, which increase the product yield.[19,41] The current understanding of the underlying mechanisms of mechanochemical reactions yielding organic cocrystals and other types of mechanochemical reactions has been recently reviewed.[16,18,19] In all mechanisms, an increased mobility of species relative to the crystalline state affording the chemical reactions observed has to be addressed.[19] Friščić et al. proposed essentially three generic mechanisms for organic cocrystallization involving different types of intermediate phases;[16,18] those are: (i) *molecular diffusion* involving the

transport of reactant molecules across surfaces, through a vapor phase (e.g., one reactant has a considerable vapor pressure) or through the crystal bulk; (ii) formation of a *liquid eutectic intermediate phase*, common in mechanochemical reactions of organic materials where covalent bond formation occurs;[16] and (iii) formation of an *amorphous intermediate phase*.

The small volumes of liquid added in LAG reactions facilitate mass transport within the mechanochemical reaction mixtures. LAG can induce mechanochemical reactivity in otherwise unreactive systems,[16−18] it increases the reaction rates,[15−20] and it can lead to the selective formation of a particular product polymorph.[16−20] For the latter 'templating' effect, a unique explanation of the liquid-phase role in LAG does not exist, and is likely to vary from reaction to reaction.[18]

Pure phases of the black and green TTF-CA polymorphs have been previously obtained from the brown form of TTF by kneading (or LAG) with water and acetone, respectively.[24] The polymorphic purity of the brown TTF powder was checked by XRPD (Figure S1 SI). We have observed that the orange TTF polymorph transforms to the brown form by neat grinding for 10 min (Figure S3 SI). The orange TTF polymorph was identified from slightly chopped crystallites (Figure S4 SI).

Since we started to study the mechanochemical synthesis of TTF-CA, we have noted that the effectiveness of certain solvents toward the formation of the black TTF-CA depends on the volume of solvent used per mass of reactants. Thus, to study the LAG solvent effect we have used the η parameter,[17] defined as microliters of solvent used per milligrams of sample ground.

A series of syntheses with increasing η were carried out from the orange and brown TTF forms by grinding with water and DMSO. The threshold η values which yielded the pure black TTF-CA polymorph are summarized in Table 2.

Table 2. Threshold η Values That Yielded the Pure Black TTF-CA Polymorph from the Orange and Brown TTF Forms Using Water and DMSO in LAG Reactions

	η (μL/mg) for water	η (μL/mg) for DMSO
brown TTF	4	4
orange TTF	2	0.02

For the orange TTF, we estimate that a minimum $\eta = 2$ μL/mg is required to synthesize the black form as a single phase using water (Figure S9c SI). For $\eta = 0.5$ μL/mg, the green TTF-CA polymorph was only identified by XRPD (Figure S9a SI), and a bright-yellow color was observed at early stages in the reaction mixture, which later became green. Under these low η conditions, it seems that the reaction could proceed similarly to neat grinding, for which the green TTF-CA is obtained as a product (from both TTF polymorphs), and a yellow intermediate color is also observed after ~5 min of the beginning of grinding, which later turns into a green color easily identifiable at around 10 min after start of grinding. The XRPD pattern of neat orange TTF and CA ground for ~5 min (Figure S10 SI) shows peaks of the brown and orange TTF, but a reaction intermediate was not identified.

For LAG with water, the samples where the black TTF-CA was identified (as pure phase or in polymorphic mixtures) showed instead a mustard-brown intermediate color. The black TTF-CA was obtained as a pure phase from the brown TTF at a slightly large $\eta = 4$ μL/mg (Figure S11b SI).

The results of LAG syntheses with DMSO from both TTF polymorphs (see Table 2) indicate that a minimum $\eta = 4$ μL/mg is necessary to obtain the black form as pure phase from the brown TTF, but $\eta = 0.02$ μL/mg could give rise to it from the orange TTF. The XRPD patterns of the TTF-CA products from the orange and brown TTF at increasing η are shown in Figure S12 SI. In most cases, DMSO still remains in the reaction mixture at the end of grinding, for which the products were left to dry in the fumehood under air. A decomposition reaction likely generated the impurity peaks observed (Figure S12 SI), which were tentatively assigned to TTF Cl$_{0.67}$.[44]

These results suggest that a different physicochemical property (or a combination of properties) of the orange TTF polymorph facilitates the formation of the black TTF-CA, observed at smaller η values, grinding with water and DMSO. We also point out that mechanochemical reactions do not happen in the bulk but in points such as lattice defects and moving cracks;[41,42] thus, other properties such as stress/strain and crystallite size of the particular powder specimens used can also play a role. Unlike the brown TTF (see Figure S2a SI), the orange TTF is made of columnar stacks of TTF molecules running along the b-axis (see Figure S5a SI), with TTF−TTF distance of 3.624 Å. This structural feature could favor the black TTF-CA product, which possesses similar columns containing TTF radical cation dimers, wherein the intradimer distance between TTF planes is 3.27(1) Å. The relation between both columnar stacks is shown in Figure S13a SI. Although the relative orientation of TTF units is different in both stacks, the conversion would require ionization and dimerization of TTF from the columns in the orange TTF and reorientation of the TTF dimers forming the columns in TTF-CA.
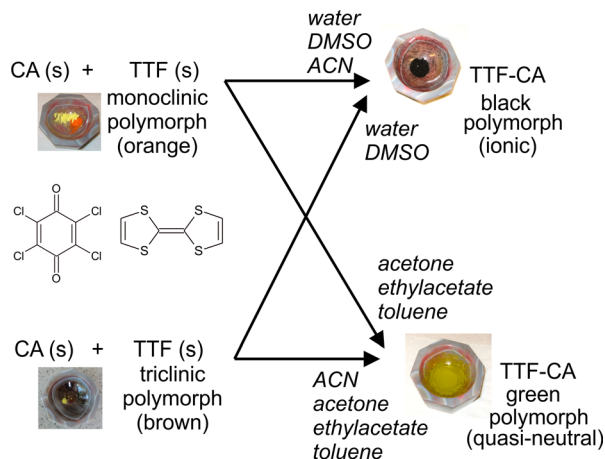
Indexing the faces of an orange TTF crystallite (Figure S6 SI) indicated that its longest axis is parallel to the b-axis; thus, this result supports the ideas above since columns of TTF are available for reaction in the largely exposed (001) and (100) faces (Figures S6 and S13b in SI). Thus, the combination of the crystal habit and the crystal structure of the orange TTF are likely to favor the formation of the black TTF-CA form.

The effect of the remaining LAG solvents toward the formation of the green or black TTF-CA polymorphs is reported for syntheses with $\eta = 4$ μL/mg, since insufficient solvent quantities could produce polymorphic mixtures, and $\eta = 4$ μL/mg seems to be above a threshold that would yield the black TTF-CA from both TTF polymorphs in the LAG reactions discussed above. The remaining solvents (except toluene) have boiling points lower than those of water and DMSO, and presumably $\eta = 4$ μL/mg would be sufficient to ensure all solvents remain in the reaction mixture during the 30-min grinding period. This issue was not quantitatively studied.

The XRPD patterns of the LAG products from both TTF forms using toluene, ethyl acetate and acetone as well as neat grinding, indicate that the quasi-neutral green TTF-CA polymorph is obtained (Figure S14 SI). Interestingly, grinding with MeCN yielded only the green form of TTF-CA from the brown TTF (at $\eta = 4$ μL/mg, $\eta = 6$ μL/mg and even $\eta = 8$ μL/mg, see Figure S15 SI), but it was able to produce the black form (at $\eta = 4$ μL/mg) from the orange TTF (Figure S14a SI), for which we concluded that for MeCN both TTF forms can yield a different polymorph of TTF-CA. Moreover, $\eta = 4$ μL/mg seems to be above the threshold value for which MeCN yields the black TTF-CA from the orange TTF, and polymorphic mixtures or the green TTF-CA will be produced

at lower η values. The effect of the six LAG solvents is summarized in Scheme 1.

[a]The threshold η values yielding the black TTF-CA from the orange TTF were 2 μL/mg (for water) and 0.02 μL/mg (for DMSO); $\eta = 4$ μL/mg yielded the black TTF-CA from this polymorph and MeCN, whereas only the green form was obtained from the brown TTF (at η = 4, 6, and 8 μL/mg). The remaining LAG syntheses were carried out at $\eta = 4$ μL/mg.

This chemical system has been particularly studied due to the very different green and black colors of both TTF-CA polymorphs[24] (see Scheme 1), which could provide visual clues about the phases formed during and after grinding. On the basis of the visual observation of the reaction mixture color during manual grinding, we have noted for LAG with organic solvents (except the MeCN reaction at $\eta = 4$ μL/mg from the orange TTF) that the green polymorph seems to be formed in the order of seconds after the start of grinding, when the pastes become homogeneous to the naked eye. After continuous grinding with sufficient volumes of water or DMSO, a brown color can be seen in the mixture (similar to mustard for water and darker for DMSO), suggesting the start of nucleation for the black form. The brown color darkens through the grinding process, and at the end of it the mixture is very dark brown or black. On occasions not reported here a black color has been observed in the powders ground with DMSO days after the grinding process finished yielding a green powder. This suggests that the solvents may remain in the ground powder and the reaction may continue at some extent after grinding has finished. Using acetone, ethyl acetate and toluene, the pastes remain green, and their XRPD patterns indicate that the green form of TTF-CA has been formed.

These observations also suggest that the presence of the liquid phase increases the reaction rates in comparison with neat grinding (for which a green color is observed at around 10 min after start of grinding), yielding pastes possibly containing supersaturated solutions[19] of the green TTF-CA polymorph and small crystallites of the solids.

Previous studies have found increased mechanochemical reactivity of materials that can dissolve in the LAG solvents, suggesting that solvation effects can be significant.[16,19] Since the estimated water solubilities[45] of TTF and CA are very low (630

mg/L and 319 mg/L, respectively) but they are soluble in the organic solvents, the increase in the reaction rates by LAG is not entirely explained by a high solubility of the reactants in the LAG solvents.

Toward explaining this rate increase, Bowmaker[19] has shown that the factors determining mass transport by diffusion in LAG vary with $1/d$,[3] where d is the particle size. Reduction in particle size by grinding would translate into an increase in reaction rates. The presence of the liquid phase dissolving one or more of the reactants increases the diffusion rates of molecules from reactants to products, and this effect rapidly increases with the decrease in reactant particle size due to grinding.[19]

Although we have not studied quantitatively the rate increase with water or the organic solvents, grinding with water also accelerates this reaction. For example, for $\eta = 2$ μL/mg, a brown color could be observed in the reaction mixture at around 4 min after start of grinding. If the reaction rate is determined by the formation of product in the solvent and diffusion of the dissolved product to a solid product phase, since the ionic product is likely to be soluble in water, this could tentatively explain the increased rates using water despite the low solubility of the reactants in it.

Moreover, the templating effect of water, DMSO and MeCN toward the formation of the black TTF-CA involves TTF reactant and solvent properties other than solubilities in the solvent series. To further investigate the templating role of those solvents toward the formation of the black (ionic) TTF-CA, we show in Table 3 the polarity index and boiling points of the solvents in the series.

Table 3. Polarity Index and Boiling Points of the Solvents in the Series

solvent	polarity index[a]	boiling point (°C)
water	9	100
DMSO	6.5	189
MeCN	6.2	81.6
acetone	5.4	56.2
ethyl acetate	4.3	77
toluene	2.3	110.6

[a]Reference 46.

The two solvents of higher polarity index and boiling point (water and DMSO), allow the formation of the black TTF-CA form from both TTF polymorphs. Those solvents could stabilize the TTF$^{+\bullet}$ and CA$^{-\bullet}$ radical ions or dissolve the ionic product. Forming the black TTF-CA involves ionizing all TTF and CA molecules (possibly from an initial quasi-neutral green phase where approximately one in three molecules is ionized), and the aggregation in the crystal packing corresponding to the black (ionic) TTF-CA. These processes would seem not as favorable for less polar solvents, and only the quasi-neutral green polymorph is obtained.

For grinding the orange TTF with MeCN at $\eta = 4$ μL/mg, we speculate that the combination of crystal structure and habit of the crystallites and the intermediate polarity of MeCN (see Table 3) allows still the formation of the black TTF-CA. For toluene, for which an initial brown color was also observed at $\eta = 4$ μL/mg, the lower polarity of the solvent would preclude the ionization of all TTF and CA molecules and the species responsible for the brown color formed upon initial cracking the orange TTF crystals would be rather disintegrated by the grinding process.

TTF-CA could also be obtained by vapor digestion (VD). In these experiments we assume the vapor pressure of the solvent remains essentially constant during the ten days reaction time, although the TTF and CA reactivity is not increased by addition of mechanical energy and formation of lattice defects, and the diffusion of species in the reaction mixture is substantially reduced in comparison to LAG.

There are fewer examples of vapor digestion reactions in the literature compared to those for LAG,[19,47−49] and detailed reaction mechanisms have not been postulated;[19] however, it is thought that the underlying mechanisms are likely related to the mechanochemical ones. For example, Braga et al.[49] report the formation of two cocrystal stoichiometries for the VD products of $[Fe(\eta^5\text{-}C_5H_4\text{-}C_5H_4N)_2]$ and pimelic acid in presence of four protic and five aprotic solvents. The authors conclude that the protic or aprotic property of the solvents and the solubility of the reactants in the layer around the crystallites determine the stoichiometry of the cocrystals found.

Solvent vapor molecules come into contact with solid reactants; for example, H atoms in rac-2,29-dihydroxy-1,19-binaphthyl have been shown to be exchanged by D atoms from CH_3OD vapors.[47] It seems reasonable that solvent vapors reach the crystallites of the TTF and CA reactants, wherein phases in which molecules have higher mobility must be formed. These mobile phases are in contact (at least at crystallite surfaces), where they can react yielding TTF-CA.

Molecular diffusion has been pointed out as controlling the formation of products in the LAG and VD synthesis of 1,1′-dipyridyl-ferrocene and anthranilic acid cocrystals.[48] This seems also valid for TTF-CA, and minimum reactant mobility and in general increasing reaction rates can be achieved by contact with solvent vapors, neat grinding and LAG, being the VD rates likely limited by the mass transport processes allowed by the VD conditions.

One significant issue to investigate using LAG and VD experiments combined is if the polymorph control effect of LAG solvents previously described would be still observed in the VD syntheses, so it could be possibly associated to intrinsic properties of each solvent (e.g., polarity index, boiling point, etc.), in combination (or not) with TTF polymorphism and crystal habits. As for LAG, high solvent polarity could favor a mechanism through which all reactant molecules are ionized, leading to the black (ionic) TTF-CA form. Moreover, cases of different polymorph reactivity with gases have been reported,[50] and different reaction products from each TTF polymorph could be observed in VD, where each TTF crystal form could act as a slightly different solid state reactant.

To further investigate the solvent effect in VD syntheses, we performed twelve VD experiments using the same solvent series combined with each TTF polymorph. The VD products are usually heterogeneous phases, with differently colored regions and even crystallites of the reactants visible to the naked eye. The crystal phases present in the laboratory or synchrotron XRPD patterns of the VD products were identified (see SI), and they are summarized in Table 4.

The analysis of these results indicates that the solvent effect observed in reactions from the brown TTF is essentially analogous to that seen in the LAG reactions. Only water and DMSO, the most polar solvents, yielded the black TTF-CA (the green TTF-CA was obtained as a minority phase with DMSO). However, from the orange TTF, VD results indicate that the black TTF-CA could also be obtained in polymorphic mixtures from all solvents used, again indicating that the black

Table 4. Solvents Used in VD Reactions and the Corresponding Crystalline Phases Identified by XRPD in VD Products from the Orange and Brown TTF Forms; Figures Indicated in the Footnotes Show the XRPD Patterns of the Reaction Products

solvent	crystal phases from VD of the brown TTF	crystal phases from VD of the orange TTF
water	**black TTF-CA**, TTF, CA ([a])	**black TTF-CA**, TTF, CA, **green TTF-CA** ([g])
DMSO	**black TTF-CA**, TTF, CA, TTFCl$_{0.67}$, **green TTF-CA** ([b])	**black TTF-CA**, TTF, CA, **green TTF-CA** ([h])
MeCN	**green TTF-CA**, TTF, CA ([c])	**black TTF-CA**, **green TTF-CA**, TTF, CA, ([i])
acetone	**green TTF-CA**, TTFCl$_{0.67}$ ([d])	**black TTF-CA** ([j])
ethyl acetate	**green TTF-CA** ([e])	**green TTF-CA**, **black TTF-CA** ([k])
toluene	**green TTF-CA**, TTF, CA ([f])	**green TTF-CA**, **black TTF-CA**, TTF ([l])

[a]Figure S16 (SI). [b]Figure S17 (SI). [c]Figure S18 (SI). [d]Figure S19 (SI). [e]Figure S20 (SI). [f]Figure S21 (SI). [g]Figure S22 (SI). [h]Figure S23 (SI). [i]Figure S24 (SI). [j]Figure S25 (SI). [k]Figure S26 (SI). [l]Figure S27 (SI).

TTF-CA is more easily obtained from the orange TTF. In VD, certainly the crystalline arrangement in the orange TTF crystallites is not perturbed by addition of mechanical energy, possibly transforming it into the brown TTF. Thus, the VD results above can be also tentatively explained by the crystal structure and crystal habit of the orange TTF, exposing columns of TTF molecules as previously discussed (Figures S13 and S6 SI), which would readily yield the black TTF-CA. Moreover, in VD reactions of the orange TTF the structural/habit effects seem to partially offset the polarity index effect, which is more significant in the VD reactions of the brown TTF and in LAG reactions, since for the latter the grinding process disrupts the orange TTF features that facilitate the formation of the black TTF-CA polymorph.

■ CONCLUSIONS

In summary, we have synthesized the black polymorph of TTF-CA by two "green chemistry" routes, LAG and VD, which considerably reduce the use of reaction solvents and for which the understanding of the reaction mechanisms is rather limited. Product polymorph control is sought in many research areas. The study of the 'templating' solvent effect in both synthetic methods toward the formation of a particular TTF-CA polymorph has been tentatively explained as a combined effect of the solvent polarity index, the crystal structures, and the crystal habits of both TTF polymorphs. A large polarity index of the solvents used, as well as columns of TTF molecules largely exposed in the faces of the orange TTF crystallites, promote the formation of the black (ionic) TTF-CA polymorph.

The crystal structure of the black polymorph of TTF-CA was determined at 298 and 20 K, confirming that this material contains $(TTF^{+\bullet})_2$ and $(CA^{-\bullet})_2$ radical ion dimers. This TTF-CA polymorph is thermodynamically more stable than the green form of TTF-CA and does not undergo a crystal phase transition in the temperature interval 298−20 K. A few crystal structure−physical properties relationships were formulated. Magnetic susceptibility data at RT further confirm the material is diamagnetic, as expected from the chemical bonding in the $(TTF^{+\bullet})_2$ and $(CA^{-\bullet})_2$ radical ion dimers, whereas the FT-IR spectra at RT and 10 K confirm that the compound remains

ionic in the temperature interval studied. The FT-IR absorption border and the analysis of the transmission spectrum indicate that TTF-CA (black form) is a semiconductor with a band gap of ~0.198 eV. The latter is in good agreement with electronic structure calculations showing minimum indirect and direct band gaps of 0.08 and 0.12 eV, respectively, and also indicating that the states immediately below the Fermi level correspond to CA units, while the ones immediately above it correspond to TTF.

■ ASSOCIATED CONTENT

ⓢ Supporting Information

Additional experimental details of the LAG syntheses, XRPD data and figures of the crystal structures of both TTF polymorphs, XRPD of the VD and additional LAG products, Rietveld refinement details, graphs, and the crystallographic information files at RT and 20 K (also deposited in the Cambridge Structural Database, CCDC 908011 and 947975 respectively). This material is available free of charge via the Internet at http://pubs.acs.org.

■ AUTHOR INFORMATION

Corresponding Author
*Telephone: +1-757-269-5732. E-mail: spagol@wm.edu.

Present Address
&Saul H. Lapidus, X-ray Science Division, Advanced Photon Source, Argonne National Laboratory, Argonne, Illinois 60439, United States.

Notes
The authors declare no competing financial interest.

■ ACKNOWLEDGMENTS

■ ABBREVIATIONS

TTF, tetrathiafulvalene; CA, chloranil; CTS, charge transfer salts; LAG, liquid assisted grinding; VD, vapor digestion; RT, room temperature; FA, fluoranil; BA, bromanil; IA, iodanil; DDQ, 2,3-dichloro-5,6-dicyano-*p*-benzoquinone; XRPD, X-ray powder diffraction; FT-IR, Fourier transform infrared spectroscopy; DFT, density functional theory; HSE06, Heyd-Scuseria-Ernzernhof

■ REFERENCES

(1) Bernstein, J. *Polymorphism in Molecular Crystals*; Clarendon Press: Oxford, 2002; pp 188−197.

(2) Braga, D.; Grepione, F.; Guy Orpen, A. *Crystal Engineering: From Molecules and Crystals to Materials*; Kluwer Academic Publishers, Dordrecht, 1999; pp 279−294.

(3) (a) Ouahab, L.; Yagubskii, E. *Organic Conductors, Superconductors and Magnets: From Synthesis to Molecular Electronics*; Kluwer Academic Publishers: Dordrecht, 2004; pp 99−112. (b) Bryce, M. R.; Murphy, L. C. *Nature* **1984**, *309*, 119−126.

(4) Mayerle, J. J.; Torrance, J. B.; Crowley, J. I. *Acta Crystallogr.* **1979**, *B35*, 2988−2995.

(5) Matsuzaki, S.; Moriyama, T.; Onomichi, M.; Toyoda, K. *Bull. Chem. Soc. Jpn.* **1983**, *56*, 369−374.

(6) Girlando, A.; Pecile, C.; Torrance, J. B. *Solid State Commun.* **1985**, *54*, 753−759.

(7) García, P.; Dahaoui, S.; Katan, C.; Souhassou, M.; Lecomte, C. *Faraday Discuss* **2007**, *135*, 217−235.

(8) Le Cointe, M.; Lemée-Cailleau, M. H.; Cailleau, H.; Toudic, B.; Toupet, L.; Heger, G.; Moussa, F.; Schweiss, P.; Kraft, K. H.; Karl, N. *Phys. Rev. B* **1995**, *51*, 3374−3386.

(9) Horiuchi, S.; Kumai, R. *J. Am. Chem. Soc.* **1998**, *120*, 7379−7380.

(10) Matsuzaki, S.; Hiejima, T.; Sano, M. *Bull. Chem. Soc. Jpn.* **1991**, *64*, 2052−2057.

(11) García, P.; Dahaoui, S.; Fertey, P.; Wenger, E.; Lecomte, C. *Phys. Rev. B* **2005**, *72*, No. 104115.

(12) Nishizawa, J.; Tanno, T.; Oohashi, T.; Watanabe, H.; Oyama, Y. *Synth. Met.* **2008**, *158*, 278−282.

(13) Girlando, A.; Marzola, F.; Pecile, C.; Torrance, J. B. *J. Chem. Phys.* **1983**, *79*, 1075−1085.

(14) Dressel, M. *Naturwissenschaften* **2007**, *94*, 527−541.

(15) Shan, N.; Toda, F.; Jones, W. *Chem. Commun.* **2002**, 2372−2373.

(16) James, S. L.; Adams, C. J.; Bolm, C.; Braga, D.; Collier, P.; Friščić, T.; Grepioni, F.; Harris, K. D. M; Hyett, G.; Jones, W.; Krebs, A.; Mack, J.; Maini, L.; Guy Orpen, A.; Parkin, I.; Shearouse, W. C.; Steed, J. W.; Waddell, D. C. *Chem. Soc. Rev.* **2012**, *41*, 413−447.

(17) Friščić, T. *J. Mater. Chem.* **2010**, *20*, 7599−7605.

(18) Friščić, T.; Jones, W. *Cryst. Growth Des.* **2009**, *9*, 1621−1637.

(19) Bowmaker, G. A. *Chem. Commun.* **2013**, *49*, 334−348.

(20) Trask, A. V.; Jones, W. *Top Curr. Chem.* **2005**, *254*, 41−70.

(21) Pagola, S.; Stephens, P. W. *J. Appl. Crystallogr.* **2010**, *43*, 370−376.

(22) Coehlo, A. *TOPAS-Academic*, 2007; v *4.1*. Available at http://www.topas-academic.net/

(23) Visser, J. *J. Appl. Crystallogr.* **1969**, *2*, 89−95.

(24) Benjamin, S.; Pagola, S.; Huba, Z.; Carpenter, E.; Abdel-Fattah, T. *Synth. Met.* **2011**, *161*, 996−1000.

(25) Larson, A. C.; Von Dreele, R. B. *Los Alamos Natl. Lab. Rep. LAUR* **2004**, 86−748.

(26) Scott, H. G. *J. Appl. Crystallogr.* **1983**, *16*, 159−163.

(27) Macrae, C. F.; Bruno, I. J.; Chisholm, J. A.; Edgington, P. R.; McCabe, P.; Pidcock, E.; Rodriguez-Monge, L.; Taylor, R.; van de Streek, J.; Wood, P. A. *J. Appl. Crystallogr.* **2008**, *41*, 466−470.

(28) Heyd, J.; Scuseria, G. E.; Ernzerhof, M. *J. Chem. Phys.* **2003**, *118*, 8207−8215.

(29) Paier, J.; Marsman, M.; Hummer, K.; Kresse, G.; Gerber, I. C.; Ángyán, J. G. *J. Chem. Phys.* **2006**, *124*, 154709.

(30) Heyd, J.; Scuseria, G. E.; Ernzerhof, M. *J. Chem. Phys.* **2006**, *124*, 219906−219901.

(31) Perdew, J. P.; Burke, K.; Ernzerhof, M. *Phys. Rev. Lett.* **1996**, *77*, 3865−3868.

(32) Henderson, T. M.; Paier, J.; Scuseria, G. E. *Phys. Status Solidi B* **2011**, *248*, 767−774.

(33) Blöchl, P. E. *Phys. Rev. B* **1994**, *50*, 17953−17979.

(34) (a) Kresse, G.; Furthmuller, J. *Comput. Mater. Sci.* **1996**, *6*, 15−50. (b) Kresse, G.; Joubert, D. *Phys. Rev. B* **1999**, *59*, 1758−1775.

(35) Spek, A. L. *Acta Crystallogr.* **2009**, *D65*, 148−155.

(36) Allen, F. H. *Acta Crystallogr.* **2002**, *B58*, 380−388.

(37) Fourmigué, M.; Batail, P. *Chem Rev* **2004**, *104*, 5379−5418.

(38) Molčanov, K.; Kojić-Prodić, B.; Babić, D.; Žilić, D.; Ravkin, B. *CrystEngComm* **2011**, *13*, 5170−5178.

(39) Mayerle, J. J.; Torrance, J. B. *Bull. Chem. Soc. Jpn.* **1981**, *54*, 3170−3172.

(40) Burger, A.; Ramberger, R. *Mikrochim. Acta II* **1979**, 259−271.

(41) Todres, Z. V. *Organic Mechanochemistry and Its Practical Applications*; CRC Taylor & Francis:NY, 2006; pp 1−10.

(42) Fernández-Bertran, J. F. *Pure Appl. Chem.* **1999**, *71*, 581−586.

(43) Baláž, P. *Int. J. Miner. Process.* **2003**, *72*, 341−354.

(44) Williams, R.; Ma, C. L.; Samson, S.; Khanna, S. K.; Somoano, R. B. *J. Chem. Phys.* **1980**, *72*, 3781−3788.

(45) *Chemspider.* The free chemical database. RSC. Available at http://www.chemspider.com/. Solubility data of TTF: CSID:89848, http://www.chemspider.com/Chemical-Structure.89848.html (accessed 02:53, Jun 28, 2013). Solubility data of CA: CSID:8068, http://www.chemspider.com/Chemical-Structure.8068.html (accessed 02:56, Jun 28, 2013).

(46) Schirmer, R. E. *Modern Methods of Pharmaceutical Analysis*, 2nd ed.; CRC Press: Baton Rouge, FL, 2000; Vol. *II*, p 305.

(47) Nakamatsu, S.; Toyota, S.; Jones, W.; Toda, F. *Chem. Commun.* **2005**, 3808−3810.

(48) Braga, D.; Giaffreda, S. L.; Rubini, K.; Grepioni, F.; Chierotti, M. R.; Gobetto, R. *CrystEngComm* **2007**, *9*, 39−45.

(49) Braga, D.; Luca Giaffreda, S. L.; Grepioni, F.; Chierotti, M. R.; Gobetto, R.; Palladino, G.; Polito, M. *CrystEngComm.* **2007**, *9*, 879−881.

(50) Chen, X.; Li, T.; Morris, K. R.; Byrn, S. R. *Mol. Cryst. Liq. Cryst.* **2002**, *381*, 121−131.